Kervinen, Mikael; Ramírez-Muñoz, Jhon; Välimaa, Alpo; Sillanpää, Mika

Landau-Zener-Stückelberg Interference in a Multimode Electromechanical System in the Quantum Regime

Published in:
Physical Review Letters

DOI:
10.1103/PhysRevLett.123.240401

Published: 01/01/2019

Document Version
Publisher's PDF, also known as Version of record

Please cite the original version:
Kervinen, M., Ramírez-Munõz, J., Välimaa, A., & Sillanpää, M. (2019). Landau-Zener-Stückelberg Interference in a Multimode Electromechanical System in the Quantum Regime. *Physical Review Letters*, *123*(24), 1-7. Article 240401. https://doi.org/10.1103/PhysRevLett.123.240401

Landau-Zener-Stückelberg Interference in a Multimode Electromechanical System in the Quantum Regime

Mikael Kervinen,[1] Jhon E. Ramírez-Muñoz,[2] Alpo Välimaa,[1] and Mika A. Sillanpää[1,*]
[1]Department of Applied Physics, Aalto University, P.O. Box 15100, FI-00076 AALTO, Finland
[2]Departamento de Física, Universidad Nacional de Colombia, 111321 Bogotá, Colombia

(Received 17 September 2019; published 12 December 2019)

The studies of mechanical resonators in the quantum regime not only provide insight into the fundamental nature of quantum mechanics of massive objects, but also introduce promising platforms for novel hybrid quantum technologies. Here we demonstrate a configurable interaction between a superconducting qubit and many acoustic modes in the quantum regime. Specifically, we show how consecutive Landau-Zener-Stückelberg (LZS) tunneling type of transitions, which take place when a system is tuned through an avoided crossing of the coupled energy levels, interfere in a multimode system. The work progresses experimental LZS interference to cover a new class of systems where the coupled levels are those of a quantum two-level system interacting with a multitude of mechanical oscillators. The work opens up applications in controlling multiple acoustic modes via parametric modulation.

DOI: 10.1103/PhysRevLett.123.240401

Advances in the control over mechanical degrees of freedom have taken a great leap forward allowing one to engineer experiments where the underlying nature of the quantized vibration energy is evident [1–7]. These works predominantly utilized superconducting quantum bits combined with a variety of different types of mechanical resonators that can be accessed resonantly through the qubit in the high gigahertz frequency range. The resonators can be made with surface acoustic waves (SAW) [5,7–12], phononic crystals [6], or high overtone bulk acoustic wave resonators (HBAR) [2,13,14], with piezoelectric materials allowing for strong coupling between electric and mechanical quantities. Mechanical modes are well isolated from the electromagnetic environment, can have longer coherence times than superconducting qubits, and can support multiple modes packed more densely than with microwave cavities [15,16]. Therefore, mechanical resonators are highly appealing in quantum computing that can utilize harmonic oscillators [17–19].

In a HBAR system, the modes mostly reside in the substrate chip and hence feature diluted strain and low acoustic losses. The system exhibits a dense spectrum of acoustic modes that interact near resonance with the qubit, suggesting a possibility to manipulate the many-mode system through the qubit. One way to do the latter is to combine slow adiabatic changes and abrupt rotations of the adiabatic basis. This type of control of qubits resembles a coherent version of Landau-Zener tunneling transitions, which have been studied extensively in various two-level systems. These include superconducting qubits [20–33], nanomechanical systems [34–39], Bose-Einstein condensates [35,40,41], optical lattices [42], and other systems [43–47].

In Landau-Zener-Stückelberg (LZS) interference, the system energy levels are modulated back and forth through an avoided crossing at a frequency ω_{rf} faster than the decay rates. Earlier work on LZS physics has strongly focused on two-level systems, aside from theoretical considerations [48–54]. In the current work, we create LZS conditions in a truly multimode quantum system that consists of a qubit coupled to many oscillators. Moreover, the oscillators are acoustic modes. As a result, we obtain a way to control a hybrid multimode quantum system using low-frequency fields.

In the case of a traditional LZS interference, we consider a quantum two-level system with the energy splitting $\omega_0(\Phi)$. The splitting depends on a control parameter Φ, which can be the flux through a SQUID loop as in this work. The levels are assumed to couple at the energy Ω, resulting in the energies $\omega(\Phi) = \pm\sqrt{\omega_0^2(\Phi) + \Omega^2}$ between the ground state and the excited state of the coupled system, and the avoided crossing equal to 2Ω at the degeneracy $\omega_0 = 0$.

When the flux is swept through the avoided crossing, Landau-Zener tunneling can nonadiabatically flip the qubit state, at the probability p_{LZ}. Outside the avoided crossing, the ground and excited states acquire a dynamical phase $\varphi = \pm\frac{1}{2}\int\omega(t)dt$ during the sweep. The phase is also contributed by the Stokes phase φ_S acquired during the LZ event, given as $\varphi_S = 0$ (or $\varphi_S = \pi/4$) in the slow $p_{\mathrm{LZ}} \approx 0$ (or fast $p_{\mathrm{LZ}} \approx 1$) limit. If the sweep is repeated back and forth across the avoided crossing, the system acquires the dynamical phases $\varphi_{1,2}$ on either side. The phases can interfere constructively or destructively, resulting in oscillations of the qubit population as a function of the sweep parameters. The conditions of constructive interference, leading to enhanced population of the excited state, are [25,33,55]

$$\varphi_2 - \varphi_1 = l\pi, \tag{1a}$$

$$\varphi_2 + \varphi_S = m\pi, \tag{1b}$$

with integer l, m. Notice the arbitrary assignment of either φ_1 or φ_2 in Eq. (1b).

Now, let us consider our system that consists of a two-level system coupled to multiple bosonic fields, and how it can be understood as an extension of the two-state LZ problem. The system is described by the multimode Jaynes-Cummings (MJC) model as (we set $\hbar = 1$)

$$H_{\mathrm{MJC}} = \frac{\omega_0}{2}\sigma_z + \sum_i \omega_m^{(i)} a_i^\dagger a_i + \sum_i g_m^{(i)}(a_i\sigma_+ + a_i^\dagger\sigma_-), \tag{2}$$

where σ_z, σ_+, and σ_- represent the standard qubit operators, and a_i ($a_i^\dagger$) is the annihilation (creation) phonon operator for mode i with frequency $\omega_m^{(i)}$. Suppose that the qubit is driven with both transverse (excitation) and longitudinal (frequency modulation) classical fields: $H_x(t) = \Omega\cos(\omega_{\mathrm{ext}}t)\sigma_x$ and $H_z(t) = (A/2)\cos(\omega_{\mathrm{rf}}t)\sigma_z$, respectively. Here Ω is the excitation amplitude and $\omega_{\mathrm{ext}} \approx \omega_0$ is the excitation frequency. The full Hamiltonian is then $H(t) = H_{\mathrm{MJC}} + H_x(t) + H_z(t)$.

In the rotating frame defined by the excitation frequency, the Hamiltonian becomes

$$H = \frac{\Delta(t)}{2}\sigma_z + \frac{\Omega}{2}\sigma_x + \sum_i \Delta_i a_i^\dagger a_i + \sum_i g_m^{(i)}(a_i\sigma_+ + a_i^\dagger\sigma_-), \tag{3}$$

with the detunings $\Delta(t) = \Delta_0 + A\cos(\omega_{\mathrm{rf}}t)$, $\Delta_0 = \omega_0 - \omega_{\mathrm{ext}}$, and $\Delta_i = \omega_m^{(i)} - \omega_{\mathrm{ext}}$. The first two terms in Eq. (3) describe the regular LZS interference problem. One also uses the term photon assisted LZS interference [29,31,52], since the qubit extracts a photon from the excitation field such that its energy is redefined as $\omega_0 - \omega_{\mathrm{ext}}$.

In our current case, we are concerned of the effect of the last two terms in Eq. (3) on the LZS problem. Taking Ω to be much smaller than the other energy scales, the situation becomes that pictured in Fig. 1. It describes modulated coupled energy levels, but they are those of a qubit and an oscillator, for a given oscillator i. Moreover, the qubit exhibits a similar coupling to many nondegenerate oscillators. In a recent experimental work [15], a system consisting of a qubit coupled to many electromagnetic cavities was used showing stimulated vacuum Rabi oscillations, but the LZS limit was not treated.

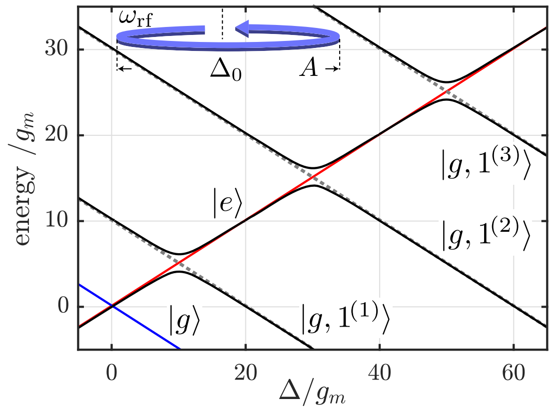

FIG. 1. Photon-assisted Landau-Zener-Stückelberg interference in a multimode qubit-oscillator system. The solid lines represent eigenvalues from Eq. (3). We restrict for simplicity to the lowest excitation manifold; for example, $|g, 1^{(3)}\rangle$ means that the qubit is in the ground state, and the harmonic mode number 3 has one photon, and the rest of the oscillators are in the ground state. The arrow sketches a slow modulation of the bare qubit energy splitting represented by the blue and red lines. The dashed lines are the energies of three harmonic modes.

On top of the picture of LZS modulation, the system allows for an interpretation in terms of multiphoton transitions [56], which manifest themselves as the appearance of sidebands in the spectrum [57]. One obtains a time-independent effective Hamiltonian:

$$H_{\mathrm{eff}}^{(n,k)} = \frac{\Delta_0 + n\omega_{\mathrm{rf}}}{2}\sigma_z + \sum_i(\Delta_i + k\omega_{\mathrm{rf}})a_i^\dagger a_i + \sum_i g_m^{(i)} J_{n-k}\left(\frac{A}{\omega_{\mathrm{rf}}}\right)(\sigma_+ a_i + \sigma_- a_i^\dagger) + \frac{\Omega}{2} J_n\left(\frac{A}{\omega_{\mathrm{rf}}}\right)\sigma_x. \tag{4}$$

$H_{\mathrm{eff}}^{(n,k)}$ describes the interaction between the nth-order sideband of the qubit and kth-order sidebands of all the mechanical modes. The nth-order sideband of the qubit interacts with the kth-order sideband of a mechanical mode i with coupling strength $g_{\mathrm{eff}}^{n-k} = g_m^{(i)} J_{n-k}(A/\omega_{\mathrm{rf}})$, where J_j are the Bessel functions of the first kind and order j. In other words, the qubit and one of the detuned mechanical modes take photons from the longitudinal field such that they become resonant and thus interact with each other at a rate g_{eff}^{n-k}.

To simulate the experimental results, we use Eq. (4) and determine the qubit population at the steady state by solving the Lindblad master equation including qubit losses, and limit the Hamiltonian to the first excitation manifold where only the zero and the one-phonon Fock states are considered [58]. This is well justified because the mechanical resonator is already in the ground state and the

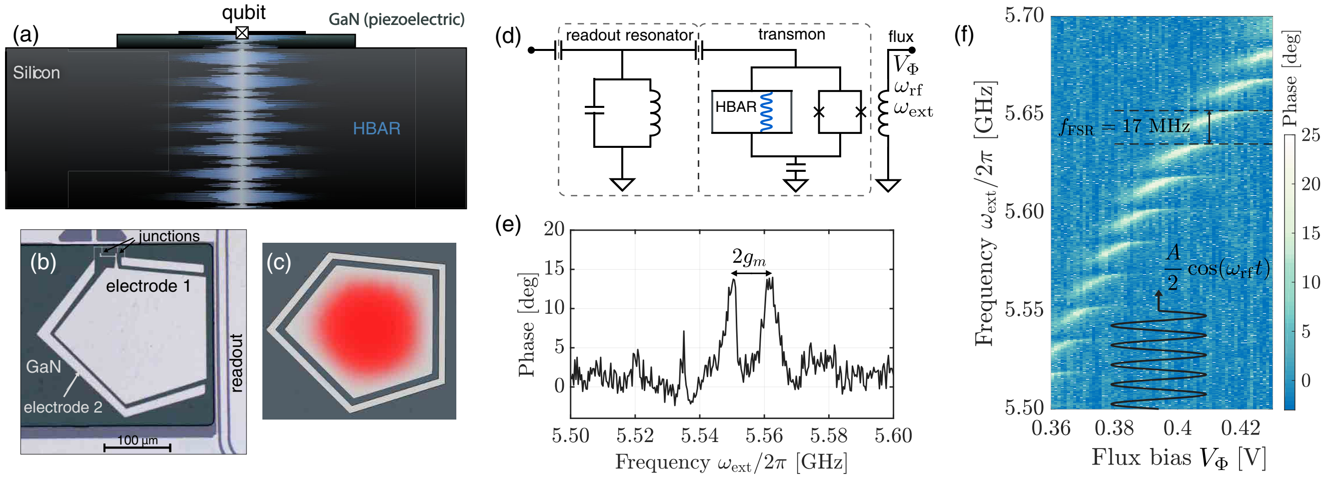

FIG. 2. (a) Schematic cross section of the high-overtone bulk acoustic modes that are located inside the massive substrate. (b) Photograph of the device shows a transmon qubit that has an irregular pentagon shape. (c) Simulation of the mode displacement profile of one overtone acoustic mode. (d) Circuit diagram of the hybrid system. The piezoelectric GaN is effectively sandwiched between the capacitor plates of the transmon. (e) Two-tone spectroscopy showing the vacuum Rabi splitting in the qubit on resonance with a mechanical mode number $i = 319$ at $\omega_0/2\pi \simeq 5.554$ GHz and flux $V_\Phi = 0.37$ V. (f) Spectroscopy as a function of flux bias, and a sketch of the slow bias modulation.

qubit excitation amplitude is small in comparison with its linewidth.

In the experiment, our device consists of a flux-tunable transmon qubit coupled to an acoustic resonator (HBAR) whose piezoelectric effect enables a strong interaction between the electric fields of the qubit and the acoustic waves of the resonator. In contrast to other work using AlN [2,13], our sample is fabricated on an epitaxial gallium nitride (GaN) coated Si substrate. The piezoelectric GaN film has been etched away everywhere else except directly under the qubit [Fig. 2(a)]. As seen in Figs. 2(b)–2(c), our transmon qubit has an asymmetric "pentamon" geometry with no parallel sides to greatly suppress lateral spurious modes of the acoustic resonator. The device is measured at the base temperature of a dilution refrigerator, where both the qubit and the high GHz frequency mechanical modes reside naturally in their quantum ground state.

The qubit has on-chip flux bias line that is connected to a bias T, enabling to set the qubit frequency (control voltage V_Φ), as well as to apply the excitation and modulation fields through the rf port [Fig. 2(d)]. The qubit-HBAR hybrid is coupled to a quarter-wavelength coplanar waveguide resonator that allows us to measure it using standard circuit QED protocols [59]. The phase of the reflected probe field signals the qubit excited state population p_e. The qubit spectrum is shown in Figs. 2(e)–2(f). The qubit experiences avoided crossings spaced by the free spectral range $\omega_{\rm FSR}/2\pi = (v/2T) \simeq 17.4$ MHz of the acoustic modes. The latter is determined by the thickness of the substrate $T \simeq 270$ μm and the acoustic velocity $v \simeq 9400$ m/s. The interaction strength between the qubit and a single acoustic mode is $g_m/2\pi \approx 5.5$ MHz interpreted from the vacuum Rabi splitting in Fig. 2(e). With the total qubit linewidth $\gamma/2\pi \approx 8$ MHz, the system is close to the strong coupling limit. The linewidth of the acoustic modes is estimated $\kappa/2\pi < 50$ kHz [56].

Next, we park the static dc flux at one spot on the qubit energy curve where the slope of the curve is close to linear. We apply the longitudinal modulation given by $H_z(t)$ on top of the static field to modulate the qubit energy around ω_0. In Fig. 3(a), we display the behavior of the qubit population when the longitudinal modulation amplitude is varied at a fixed modulation frequency. This measurement also serves as a calibration of A, since the attenuation inside the refrigerator at finite frequencies is not well known. The qubit population is maximized around parameter regions satisfying both the interference conditions, Eqs. (1a) and (1b). The latter is clearly illustrated in Fig. 3(b), which is a simulation on a single qubit alone and hence describes the regular LZS situation. In the experimental data, however, the regions of constructive interference exhibit additional fine structure on top of the LZS interference pattern. We attribute the observed bending of the experimental data to the left in Fig. 3(a) to a combination of curvature in the qubit frequency-flux relation and a flux drift during the measurement.

In order to describe the additional resonances in Fig. 3(b), we adopt the multiphoton picture in Eq. (4). The multiphoton transitions involve both the qubit and each mechanical mode. For example, when the transverse driving field satisfies the condition $\Delta_i + k_i\omega_{\rm rf} = \Delta_j + k_j\omega_{\rm rf}$, two mechanical modes i and j become resonant [60]. The case is extended to any number of modes. Moreover, if the effective qubit splitting $\frac{1}{2}(\Delta_0 + n\omega_{\rm rf})$ also satisfies the equality, the qubit is also on resonance with them. In Fig. 4(a) we display the latter situation. Three

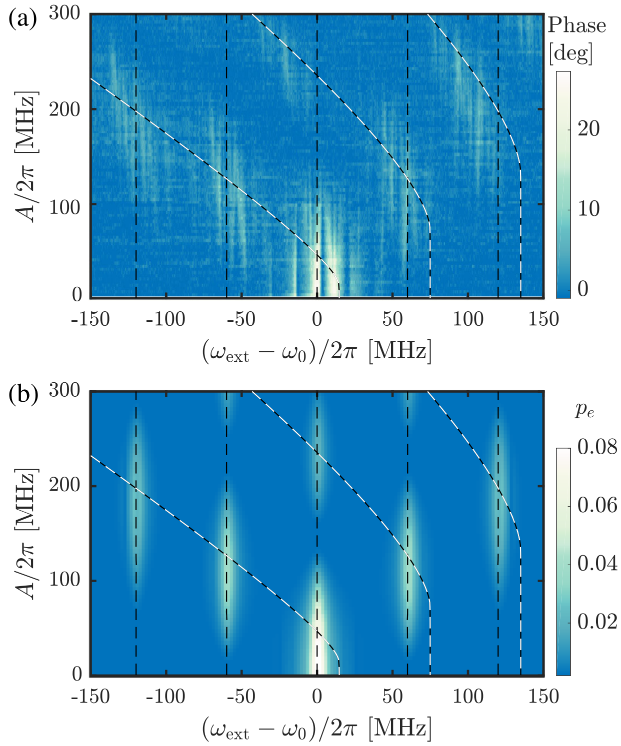

FIG. 3. LZS dynamics in the multimode electromechanical system. (a) Experimental data depicting the qubit population when the slow modulation amplitude is varied. (b) Simulation of the qubit population *without* presence of the acoustic modes in an otherwise similar situation. In both (a) and (b), the dashed black (black-white) lines display the respective LZS resonance conditions [Eq. (1a), Eq. (1b)]. The modulation frequency is $\omega_{\rm rf}/2\pi = 60$ MHz.

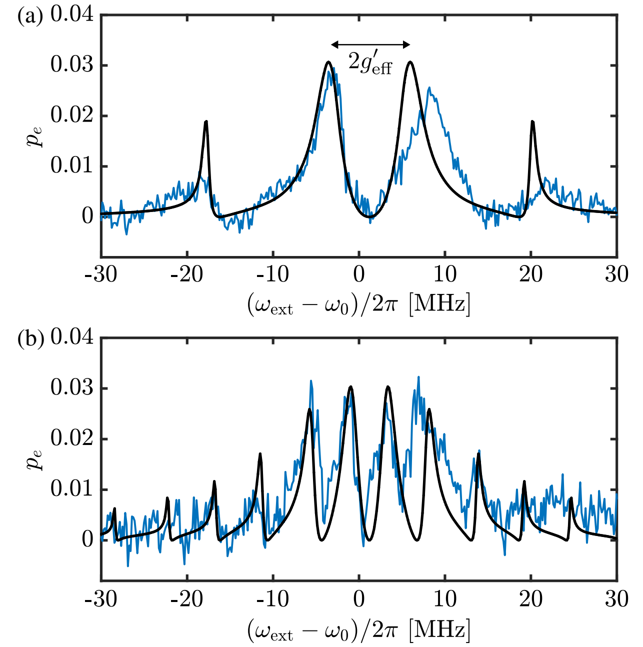

FIG. 4. Resonances in the rotating frame. (a) Excited state probability of the qubit under low-frequency modulation with $\omega_{\rm rf}/2\pi = 139$; (b) with $\omega_{\rm rf}/2\pi = 145$ MHz. In both (a),(b), the qubit frequency $\omega_0/2\pi \simeq 5.484$ GHz, flux $V_\Phi = 0.343$ V, $A/2\pi = 210$ MHz, and $\Omega/2\pi = 3$ MHz. The black solid lines are numerical simulation with $\gamma/2\pi = 8$, $g_m/2\pi = 5.5$ MHz. The vertical axis scaling from the measured phase into p_e is used as an adjustable parameter. We can infer that in (b), the sideband acoustic modes exhibit entanglement characterized by logarithmic negativity on the order 0.07.

modes $i = 307$ ($\omega_m^{(i)}/2\pi = 5.345$), $j = 323$ ($\omega_m^{(j)}/2\pi = 5.623$), and $h = 315$ ($\omega_m^{(h)}/2\pi = 5.484$ GHz) form a tripartite resonance when $\omega_{\rm rf}/2\pi = 139$ MHz $= 8 \times \omega_{\rm FSR}/2\pi$ with $k_i = 1$, $k_j = -1$, $k_h = 0$, and with the qubit at $\Delta_0 \simeq 0$ and $n = 0$. The effective vacuum Rabi splitting $\approx$11 MHz is nearly as large as seen in the nonmodulated case shown in Fig. 2(e), although the simplest expectation yields $2g_{\rm eff}^{\pm 1} \simeq 2\pi \times 6$ MHz. Instead, the vacuum Rabi splitting is that of a coresonant four partite ($N = 4$ below) system formed by three oscillators and a qubit. In the present case, the couplings $g_{\rm eff}^{\pm 1}$ and $g_{\rm eff}^{0}$ are nearly equal, and the total coupling is $2g'_{\rm eff} \approx \sqrt{N-1} \times 2g_{\rm eff}^{\pm 1} \simeq 2\pi \times 10.6$ MHz, in a good agreement with the measurement.

When the subsystems are brought off-resonant by detuning the modulation frequency as shown in Fig. 4(b), the system is understood as several detuned resonators that do not exhibit appreciable energy exchange.

The resonance conditions can be illustrated by plotting the qubit population as a function of two control parameters. In Fig. 5(a) we can observe the resolved sidebands in the spectrum at frequencies $\omega_{\rm ext} = \omega_0 \pm n\omega_{\rm rf}$ ($n = 0, 1, 2, \ldots$), see Eq. (4). The interaction is mediated to multiple acoustic modes that exhibit sidebands as well. Each mechanical mode represents a starting point for a set of sideband transitions ($\omega \approx \omega_m^{(i)} \pm k\omega_{\rm rf}$, $k = 0, 1, 2, \ldots$). They are easily identified in the measurement [Fig. 5(a)] and in the corresponding simulation [Fig. 5(b)]. At the lowest frequencies below the bias-T cutoff, the modulation does not reach the qubit, and the measurement in this region is hence equivalent to a nonmodulated system. In the central band we see diagonal anticrossings separated by the free spectral range $\omega_{\rm FSR}/2\pi = 17.4$ MHz. For example, when the modulation frequency is 130–170 MHz we see the interaction of mechanical modes $\omega_m^{(i)}$, $i = 315 \pm 8, \pm 9, \pm 10$ with the qubit, see Ref. [56]. Therefore by selecting the frequency of the modulation to match $\omega_0 - \omega_m^{(i)}$, different acoustic modes can be brought into resonance with the qubit allowing addressing and hybridizing of different modes.

We have shown that a quantum electromechanical system under frequency modulation can be understood starting from Landau-Zener-Stückelberg interference. The work enables us to selectively configure mechanical modes at mismatched frequencies to interact with the qubit. Through improvements on the qubit coherence,

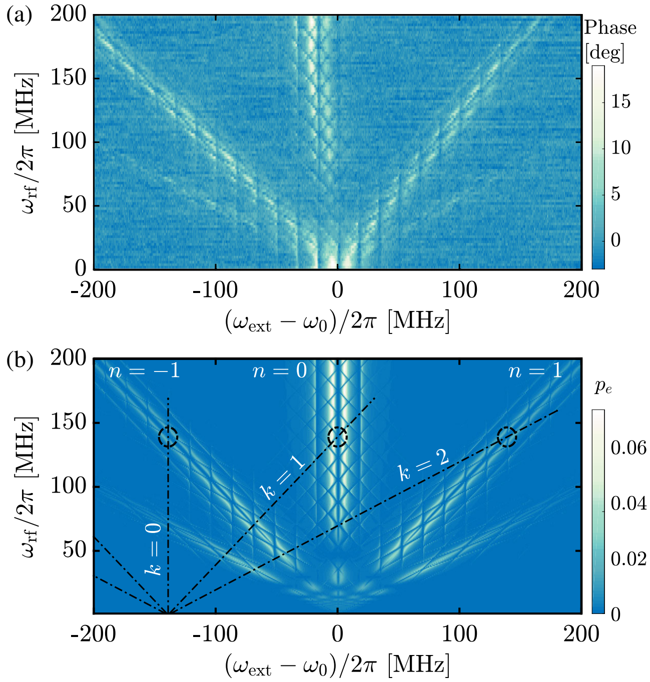

FIG. 5. Multiphoton transitions in the multimode system. (a) The measured phase shift shows how the qubit and acoustic modes experience resolved sidebands that are detuned from the original resonance by $\omega_{\rm rf}$. (b) Numerical simulation showing the qubit population. The parameters in both (a),(b) are as in Fig. 4 except $A/2\pi = 110$ MHz. The qubit sidebands are marked with n, and the mechanical sidebands as an example for $\omega_m^{(307)}/2\pi \simeq 5.345$ GHz by k.

and adjustments of the coupling [56] the approach can be useful in quantum information.

This work was supported by the Academy of Finland (Contracts No. 307757, No. 312057), by the European Research Council (Contract No. 615755), by the Centre for Quantum Engineering at Aalto University, by The Finnish Foundation for Technology Promotion, and by the Jenny and Antti Wihuri Foundation. We acknowledge funding from the European Union's Horizon 2020 research and innovation program under Grant Agreement No. 732894 (FETPRO HOT). J. E. R. M. acknowledges support from UN-DIEB project HERMES 41611, and from COLCIENCIAS under project HERMES 31361 (code 110171249692) and "Beca de Doctorados Nacionales de COLCIENCIAS 727." We acknowledge the facilities and technical support of Otaniemi research infrastructure for Micro and Nanotechnologies (OtaNano). We would like to thank Herbert Vinck Posada for helpful discussions on the theoretical calculations.

*Mika.Sillanpaa@aalto.fi

[1] A. D. O'Connell, M. Hofheinz, M. Ansmann, R. C. Bialczak, M. Lenander, E. Lucero, M. Neeley, D. Sank, H. Wang, M. Weides, J. Wenner, J. M. Martinis, and A. N. Cleland, Quantum ground state and single-phonon control of a mechanical resonator, Nature (London) **464**, 697 (2010).
[2] Y. Chu, P. Kharel, T. Yoon, L. Frunzio, P. T. Rakich, and R. J. Schoelkopf, Creation and control of multi-phonon Fock states in a bulk acoustic-wave resonator, Nature (London) **563**, 666 (2018).
[3] K. J. Satzinger, Y. P. Zhong, H. S. Chang, G. A. Peairs, A. Bienfait, M.-H. Chou, A. Y. Cleland, C. R. Conner, E. Dumur, J. Grebel, I. Gutierrez, B. H. November, R. G. Povey, S. J. Whiteley, D. D. Awschalom, D. I. Schuster, and A. N. Cleland, Quantum control of surface acoustic wave phonons, Nature (London) **563**, 661 (2018).
[4] J. J. Viennot, X. Ma, and K. W. Lehnert, Phonon-Number-Sensitive Electromechanics, Phys. Rev. Lett. **121**, 183601 (2018).
[5] L. R. Sletten, B. A. Moores, J. J. Viennot, and K. W. Lehnert, Resolving Phonon Fock States in a Multimode Cavity with a Double-Slit Qubit, Phys. Rev. X **9**, 021056 (2019).
[6] P. Arrangoiz-Arriola, E. Alex Wollack, Z. Wang, M. Pechal, W. Jiang, T. P. McKenna, J. D. Witmer, R. Van Laer, and A. H. Safavi-Naeini, Resolving the energy levels of a nanomechanical oscillator, Nature (London) **571**, 537 (2019).
[7] A. Bienfait, K. J. Satzinger, Y. P. Zhong, H.-S. Chang, M.-H. Chou, C. R. Conner, É. Dumur, J. Grebel, G. A. Peairs, R. G. Povey, and A. N. Cleland, Phonon-mediated quantum state transfer and remote qubit entanglement, Science **364**, 368 (2019).
[8] M. V. Gustafsson, T. Aref, A. F. Kockum, M. K. Ekström, G. Johansson, and P. Delsing, Propagating phonons coupled to an artificial atom, Science **346**, 207 (2014).
[9] A. Noguchi, R. Yamazaki, Y. Tabuchi, and Y. Nakamura, Qubit-Assisted Transduction for a Detection of Surface Acoustic Waves Near the Quantum Limit, Phys. Rev. Lett. **119**, 180505 (2017).
[10] R. Manenti, A. F. Kockum, A. Patterson, T. Behrle, J. Rahamim, G. Tancredi, F. Nori, and P. J. Leek, Circuit quantum acoustodynamics with surface acoustic waves, Nat. Commun. **8**, 975 (2017).
[11] A. N. Bolgar, J. I. Zotova, D. D. Kirichenko, I. S. Besedin, A. V. Semenov, R. S. Shaikhaidarov, and O. V. Astafiev, Quantum Regime of a Two-Dimensional Phonon Cavity, Phys. Rev. Lett. **120**, 223603 (2018).
[12] G. Andersson, B. Suri, L. Guo, T. Aref, and P. Delsing, Nonexponential decay of a giant artificial atom, Nat. Phys. **15**, 1123 (2019).
[13] Y. Chu, P. Kharel, W. H. Renninger, L. D. Burkhart, L. Frunzio, P. T. Rakich, and R. J. Schoelkopf, Quantum acoustics with superconducting qubits, Science **358**, 199 (2017).
[14] M. Kervinen, I. Rissanen, and M. Sillanpää, Interfacing planar superconducting qubits with high overtone bulk acoustic phonons, Phys. Rev. B **97**, 205443 (2018).
[15] R. K. Naik, N. Leung, S. Chakram, P. Groszkowski, Y. Lu, N. Earnest, D. C. McKay, J. Koch, and D. I. Schuster, Random access quantum information processors using multimode circuit quantum electrodynamics, Nat. Commun. **8**, 1904 (2017).

[16] N. M. Sundaresan, Y. Liu, D. Sadri, L. J. Szőcs, D. L. Underwood, M. Malekakhlagh, H. E. Türeci, and A. A. Houck, Beyond Strong Coupling in a Multimode Cavity, Phys. Rev. X **5**, 021035 (2015).
[17] Z. Leghtas, G. Kirchmair, B. Vlastakis, R. J. Schoelkopf, M. H. Devoret, and M. Mirrahimi, Hardware-Efficient Autonomous Quantum Memory Protection, Phys. Rev. Lett. **111**, 120501 (2013).
[18] Z. Leghtas, S. Touzard, I. M. Pop, A. Kou, B. Vlastakis, A. Petrenko, K. M. Sliwa, A. Narla, S. Shankar, M. J. Hatridge, M. Reagor, L. Frunzio, R. J. Schoelkopf, M. Mirrahimi, and M. H. Devoret, Confining the state of light to a quantum manifold by engineered two-photon loss, Science **347**, 853 (2015).
[19] C. T. Hann, C.-L. Zou, Y. Zhang, Y. Chu, R. J. Schoelkopf, S. M. Girvin, and L. Jiang, Hardware-Efficient Quantum Random Access Memory with Hybrid Quantum Acoustic Systems, arXiv:1906.11340 [Phys. Rev. Lett. (to be published)].
[20] W. D. Oliver, Y. Yu, J. C. Lee, K. K. Berggren, L. S. Levitov, and T. P. Orlando, Mach-zehnder interferometry in a strongly driven superconducting qubit, Science **310**, 1653 (2005).
[21] M. Sillanpää, T. Lehtinen, A. Paila, Y. Makhlin, and P. Hakonen, Continuous-Time Monitoring of Landau-Zener Interference in a Cooper-Pair Box, Phys. Rev. Lett. **96**, 187002 (2006).
[22] C. M. Wilson, T. Duty, F. Persson, M. Sandberg, G. Johansson, and P. Delsing, Coherence Times of Dressed States of a Superconducting Qubit Under Extreme Driving, Phys. Rev. Lett. **98**, 257003 (2007).
[23] A. Izmalkov, S. H. W. van der Ploeg, S. N. Shevchenko, M. Grajcar, E. Il'ichev, U. Hübner, A. N. Omelyanchouk, and H.-G. Meyer, Consistency of Ground State and Spectroscopic Measurements on Flux Qubits, Phys. Rev. Lett. **101**, 017003 (2008).
[24] D. M. Berns, M. S. Rudner, S. O. Valenzuela, K. K. Berggren, W. D. Oliver, L. S. Levitov, and T. P. Orlando, Amplitude spectroscopy of a solid-state artificial atom, Nature (London) **455**, 51 (2008).
[25] S. N. Shevchenko, S. Ashhab, and F. Nori, Landau–Zener–Stückelberg interferometry, Phys. Rep. **492**, 1 (2010).
[26] G. Sun, X. Wen, B. Mao, J. Chen, Y. Yu, P. Wu, and S. Han, Tunable quantum beam splitters for coherent manipulation of a solid-state tripartite qubit system, Nat. Commun. **1**, 51 (2010).
[27] G. Sun, X. Wen, B. Mao, Y. Yu, J. Chen, W. Xu, L. Kang, P. Wu, and S. Han, Landau-Zener-Stückelberg interference of microwave-dressed states of a superconducting phase qubit, Phys. Rev. B **83**, 180507(R) (2011).
[28] C. M. Quintana, K. D. Petersson, L. W. McFaul, S. J. Srinivasan, A. A. Houck, and J. R. Petta, Cavity-Mediated Entanglement Generation Via Landau-Zener Interferometry, Phys. Rev. Lett. **110**, 173603 (2013).
[29] J. Li, M. P. Silveri, K. S. Kumar, J. M. Pirkkalainen, A. Vepsäläinen, W. C. Chien, J. Tuorila, M. A. Sillanpää, P. J. Hakonen, E. V. Thuneberg, and G. S. Paraoanu, Motional averaging in a superconducting qubit, Nat. Commun. **4**, 1420 (2013).
[30] X. Tan, D.-W. Zhang, Z. Zhang, Y. Yu, S. Han, and S.-L. Zhu, Demonstration of Geometric Landau-Zener Interferometry in a Superconducting Qubit, Phys. Rev. Lett. **112**, 027001 (2014).
[31] M. P. Silveri, K. S. Kumar, J. Tuorila, J. Li, A. Vepsäläinen, E. V. Thuneberg, and G. S. Paraoanu, Stückelberg interference in a superconducting qubit under periodic latching modulation, New J. Phys. **17**, 043058 (2015).
[32] P. Neilinger, S. N. Shevchenko, J. Bogár, M. Rehák, G. Oelsner, D. S. Karpov, U. Hübner, O. Astafiev, M. Grajcar, and E. Il'ichev, Landau-Zener-Stückelberg-Majorana lasing in circuit quantum electrodynamics, Phys. Rev. B **94**, 094519 (2016).
[33] M. P. Silveri, J. A. Tuorila, E. V. Thuneberg, and G. S. Paraoanu, Quantum systems under frequency modulation, Rep. Prog. Phys. **80**, 056002 (2017).
[34] M. D. LaHaye, J. Suh, P. M. Echternach, K. C. Schwab, and M. L. Roukes, Nanomechanical measurements of a superconducting qubit, Nature (London) **459**, 960 (2009).
[35] A. Zenesini, H. Lignier, G. Tayebirad, J. Radogostowicz, D. Ciampini, R. Mannella, S. Wimberger, O. Morsch, and E. Arimondo, Time-Resolved Measurement of Landau-Zener Tunneling in Periodic Potentials, Phys. Rev. Lett. **103**, 090403 (2009).
[36] S. Gasparinetti, P. Solinas, and J. P. Pekola, Geometric Landau-Zener Interferometry, Phys. Rev. Lett. **107**, 207002 (2011).
[37] S. N. Shevchenko, S. Ashhab, and F. Nori, Inverse Landau-Zener-Stückelberg problem for qubit-resonator systems, Phys. Rev. B **85**, 094502 (2012).
[38] M. J. Seitner, H. Ribeiro, J. Kölbl, T. Faust, J. P. Kotthaus, and E. M. Weig, Classical Stückelberg interferometry of a nanomechanical two-mode system, Phys. Rev. B **94**, 245406 (2016).
[39] T. Ota, K. Hitachi, and K. Muraki, Landau-Zener-Stückelberg interference in coherent charge oscillations of a one-electron double quantum dot, Sci. Rep. **8**, 5491 (2018).
[40] J.-N. Zhang, C.-P. Sun, S. Yi, and Franco Nori, Spatial Landau-Zener-Stückelberg interference in spinor Bose-Einstein condensates, Phys. Rev. A **83**, 033614 (2011).
[41] A. J. Olson, S.-J. Wang, R. J. Niffenegger, C.-H. Li, C. H. Greene, and Y. P. Chen, Tunable Landau-Zener transitions in a spin-orbit-coupled Bose-Einstein condensate, Phys. Rev. A **90**, 013616 (2014).
[42] S. Kling, T. Salger, C. Grossert, and M. Weitz, Atomic Bloch-Zener Oscillations and Stückelberg Interferometry in Optical Lattices, Phys. Rev. Lett. **105**, 215301 (2010).
[43] M. Mark, T. Kraemer, P. Waldburger, J. Herbig, C. Chin, H.-C. Nägerl, and R. Grimm, Stückelberg Interferometry with Ultracold Molecules, Phys. Rev. Lett. **99**, 113201 (2007).
[44] J. R. Petta, H. Lu, and A. C. Gossard, A coherent beam splitter for electronic spin states, Science **327**, 669 (2010).
[45] P. Huang, J. Zhou, F. Fang, X. Kong, X. Xu, C. Ju, and J. Du, Landau-Zener-Stückelberg Interferometry of a Single Electronic Spin in a Noisy Environment, Phys. Rev. X **1**, 011003 (2011).
[46] J. Stehlik, Y. Dovzhenko, J. R. Petta, J. R. Johansson, F. Nori, H. Lu, and A. C. Gossard, Landau-Zener-Stückelberg interferometry of a single electron charge qubit, Phys. Rev. B **86**, 121303(R) (2012).

[47] L. Wang, T. Tu, B. Gong, C. Zhou, and G.-C. Guo, Experimental realization of non-adiabatic universal quantum gates using geometric Landau-Zener-Stückelberg interferometry, Sci. Rep. **6**, 19048 (2016).

[48] S. Brundobler and V. Elser, *S*-matrix for generalized Landau-Zener problem, J. Phys. A **26**, 1211 (1993).

[49] T. Usuki, Theoretical study of Landau-Zener tunneling at the $M+N$ level crossing, Phys. Rev. B **56**, 13360 (1997).

[50] N. A. Sinitsyn, Multiparticle Landau-Zener problem: Application to quantum dots, Phys. Rev. B **66**, 205303 (2002).

[51] D. Zueco, P. Hänggi, and S. Kohler, Landau-Zener tunnelling in dissipative circuit QED, New J. Phys. **10**, 115012 (2008).

[52] Z. Sun, J. Ma, X. Wang, and F. Nori, Photon-assisted Landau-Zener transition: Role of coherent superposition states, Phys. Rev. A **86**, 012107 (2012).

[53] S. Ashhab, Landau-Zener transitions in a two-level system coupled to a finite-temperature harmonic oscillator, Phys. Rev. A **90**, 062120 (2014).

[54] S. Ashhab, Landau–Zener–Stueckelberg interferometry with driving fields in the quantum regime, J. Phys. A **50**, 134002 (2017).

[55] J. Tuorila, M. Silveri, M. Sillanpää, E. Thuneberg, Y. Makhlin, and P. Hakonen, Charge qubit driven via the Josephson nonlinearity, Supercond. Sci. Technol. **26**, 124001 (2013).

[56] See Supplemental Material at http://link.aps.org/supplemental/10.1103/PhysRevLett.123.240401 for experimental and theoretical details.

[57] F. Beaudoin, M. P. da Silva, Z. Dutton, and A. Blais, First-order sidebands in circuit QED using qubit frequency modulation, Phys. Rev. A **86**, 022305 (2012).

[58] B. A. Moores, L. R. Sletten, J. J. Viennot, and K. W. Lehnert, Cavity Quantum Acoustic Device in the Multimode Strong Coupling Regime, Phys. Rev. Lett. **120**, 227701 (2018).

[59] D. I. Schuster, A. Wallraff, A. Blais, L. Frunzio, R.-S. Huang, J. Majer, S. M. Girvin, and R. J. Schoelkopf, ac Stark Shift and Dephasing of a Superconducting Qubit Strongly Coupled to a Cavity Field, Phys. Rev. Lett. **94**, 123602 (2005).

[60] The excitation and modulation frequencies are incommensurate except in vanishingly small regions in the parameter space, and hence a physical phase difference between the tones does not exist.